

**DOKUZ EYLÜL UNIVERSITY**  
**GRADUATE SCHOOL OF MINERAL PROCESSING SCIENCES**

**PRODUCTION OF MgO CATALYZOR  
NANOPARTICLES BY FLAME SPREY  
PYROLYSES METHOD**

by  
**Berkan ÖZTÜRK**

**July, 2013**  
**İZMİR**

# **PRODUCTION OF MgO CATALYZOR NANOPARTICLES BY FLAME SPREY PYROLYSES METHOD**

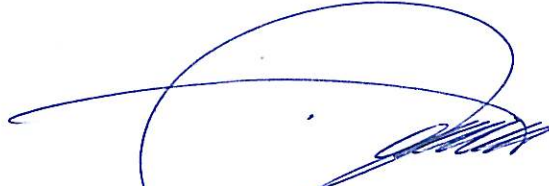
**A Thesis Submitted to the  
Graduate School of Natural and Applied Sciences of Dokuz Eylül University  
In Partial Fulfillment of the Requirements for the Degree of Master of Science  
in Mining Engineering, Applied Mineral Processing Program**

**by  
Berkan ÖZTÜRK**

**July, 2013  
İZMİR**

## M.Sc THESIS EXAMINATION RESULT FORM


We have read the thesis entitled “**PRODUCTION OF MGO CATALYZOR NANOPARTICLES BY FLAME SPREY PYROLYSES METHOD**” completed by **BERKAN ÖZTÜRK** under supervision of **PROF. DR. TURAN BATAR** and we certify that in our opinion it is fully adequate, in scope and in quality, as a thesis for the degree of Master of Science.



---

Prof. Dr. Turan BATAR


Supervisor



---

Prof. Dr. Erdal Gelik

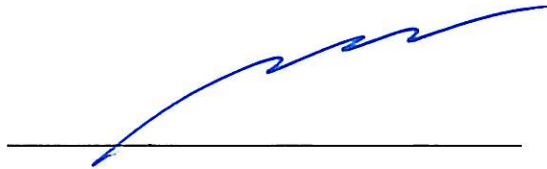
(Jury Member)



---

Y. Doç. Dr. Ömer Merme

(Jury Member)



---

Prof. Dr. Ayşe OKUR  
Director  
Graduate School of Natural and Applied Sciences

## ACKNOWLEDGMENTS

I wish to express my sincere gratitude to Prof. Turan BATAR, principal and Prof.Erdal ÇELİK, and Assistant Professor Ömer MERMER, Metallurgical and Material Department to do my project work on " PRODUCTION OF MGO CATALYZOR NANOPARTICLES BY FLAME SPREY PYROLYSES METHOD " which are. My special thanks to Orkut SANCAKOĞLU and Mustafa EROL and Baran TUFAN and Serdar YILDIRIM for helping to measure my experimental data. For their kind co-operation to the completion of my project work.

I would like to express my gratitude towards my wife İdil İpek ÖZTÜRK & my parents Fatma & İbrahim ÖZTÜRK and member of Öztürk Family (Serkan & İffet) for their kind co-operation and encouragement which help me in completion of this project.

Berkan ÖZTÜRK

# **PRODUCTION OF MgO CATALYZOR NANO PARTICLES BY FLAME SPREY PYROLYSES METHOD**

## **ABSTRACT**

Oxide nanomaterials have a wide range of applications including as catalysts and starting materials for preparing advanced structural ceramics. Magnesium oxide is highly insulating crystalline solid with sodium chloride crystal structure with excellent properties such as chemical inertness, electrical insulation, optical transparency, high temperature stability, high thermal conductivity, and secondary electron emission. In this study, nano scale magnesium oxide powders were synthesized via flame spray pyrolysis technique. The produced powders were post-annealed to obtain crystalline structure at 500 degrees centigrade for 120 minutes in air. The phase structure was analyzed by x-ray diffractometer. The morphology and accurate size of the primary particles were further investigated by scanning electron microscope. Particle size was determined using particle size analyzer. As a result of the analysis, Particles size is 121 nanometer and the phase structure is periclase magnesium oxide.

**Keywords** : Flame spray pyrolysis, nanoparticle magnezium oxide

**NANOBOYUTLU MAGNEZYUMOKSİT**  
**MgO KATALİZÖR NANOPARTİÜLLERİNİN ALEV SPREY PİROLİZ**  
**YÖNTEMİ İLE SENTEZİ**

**ÖZ**

Oksit nanomalzemeler gelişmiş yapısal seramiklerin hazırlanması için katalizör ve başlangıç malzemeleri dahil olmak üzere geniş bir uygulama alanına sahiptir. Magnezyum oksit kimyasal olarak inert, elektrik yalıtımı, optik şeffaflık, yüksek sıcaklık kararlılığı, yüksek termal iletkenlik ve ikincil elektron emisyonu gibi mükemmel özelliklere sahip olmakla birlikte sodyum klörür kristal yapısı ile son derece yalıtkan kristalin malzemedir. Bu çalışmada, nanoboyutlu magnezyum oksit tozu alev sprej piroliz tekniğı ile sentezlenmiştir. Üretilen tozlara havada 120 dakika 500 santigrad derecede kristalin yapısını elde etmek için tavlama yapılmıştır. Faz yapısı x-ışınları difraktometresi ile birincil partiküllerin morfolojisi ve boyutu taramalı elektron mikroskopunda ile incelenmiştir. Partikül büyüklüğü, partikül boyutu analizi kullanılarak belirlenmiştir. Analiz sonucunda, Partiküllerin ortalama boyutu 60 nanometredir ve faz yapısı magnezyum oksit periklas'dır.

**Anahtar Kelimeler:** Alev sprej piroliz, nanoboyutlu magnezyum oksit

## CONTENTS

	<b>Page</b>
THESIS EXAMINATION RESULT FORM .....	ii
ACKNOWLEDGEMENTS .....	iii
ABSTRACT .....	iv
ÖZ .....	v
LIST OF FIGURES .....	iix
LIST OF TABLES .....	x
<b>CHAPTER ONE – INTRODUCTION .....</b>	<b>1</b>
1.1 General .....	1
1.2 Organization of the Thesis .....	2
<b>CHAPTER TWO – THEORETICAL BACKGROUND.....</b>	<b>4</b>
2.1 Nanotechnology.....	4
2.2 Carbon Nanotube.....	7
2.3 Nanoparticle Production.....	9
2.4 Magnesium Oxide.....	11
2.5 Sol–Gel Synthesis of MgO Nanocrystallites.....	14
2.6 Flame Spray Pyrolysis Method.....	15
<b>CHAPTER THREE – EXPERIMENTAL METHOD.....</b>	<b>17</b>
3.1 Objective.....	17
3.2 Materials.....	17
3.3 Production Technique.....	17
3.4 Solution Characterization .....	27
3.4.1 Turbidimeter .....	27
3.4.2 pH meter.....	28
3.5 Material Characterization .....	29

3.5.1 Differential Thermal Analysis-Thermogravimetry (DTA-TG).....	29
3.5.2 Fourier Transform Infrared Spectroscopy (FTIR) .....	30
3.5.3 X-Ray Diffraction (XRD).....	30
3.5.4 X-ray Photoelectron Spectroscopy (XPS).....	31
3.5.5 Scanning Electron Microscopy (SEM).....	32
3.5.6 Particle Size Analysis.....	32
<b>CHAPTER FOUR – RESULT AND DISCUSSIONS .....</b>	<b>33</b>
4.1 Solution Characteristics.....	33
4.1.1 Turbidity .....	33
4.1.2 Asidic/Basic Characteristics .....	33
4.2 Material Characteristics.....	34
4.2.1 DTA-TG Analysis .....	34
4.2.2 FT-IR Results .....	35
4.2.3 Phase Analysis.....	36
4.2.4 XPS Analysis.....	36
4.2.5 Microstructure.....	39
4.2.6 Particle Size Distribution.....	41
<b>CHAPTER FIVE – CONCLUSIONS AND FUTURE PLAN .....</b>	<b>42</b>
<b>REFERENCES.....</b>	<b>45</b>



## LIST OF FIGURES

	<b>Page</b>
Figure 2.1 Illustration of some possible structures of carbon nanotubes, depending on how graphite sheets are rolled: (a) armchair structure; (b) zigzag structure; (c) chiral.....	7
Figure 2.2 Experimental arrangement for synthesizing carbon nanotubes by laser evaporation .....	8
Figure 2.3 Schematic representation of the flame spray pyrolysis process.....	15
Figure 3.1 Nozzle unit and nanopowders nozzle inside flame spray pyrolysis device.....	18
Figure 3.2 Gas and water connections to the nozzle on the Nozzle Unit internal wall: 1–nozzle cooling water outlet; 2–nozzle cooling water inlet; 3–premixed supporting flame gas; 4–dispersion oxygen; 5–sheath gas (optional); 6–capillary cooling water outlet; 7–capillary cooling water inlet.....	18
Figure 3.3 Top view of the NanoPowderNozzle with capillary and dispersion gas outlet (O), the concentric outlet gap for the premixed supporting flame gas (N) and sintered metal ring for the optional sheath gas flow (M).....	19
Figure 3.4 View of the back-side of the nano powder nozzle with connectors for the liquid feed (E), dispersion gas (D), premixed supporting flame gas (F), optional sheath gas (S), and capillary cooling water (I, K).....	19
Figure 3.5 Liquid feed shaft, consisting of the dispersion pressure regulator (G1), locking nut (G2) and liquid feed shaft o-rings (G3).....	20
Figure 3.6 Liquid feed shaft inner components necessary for the capillary cooling circuit: liquid feed capillary (O) with Luer Lock connector (E) and M2 thread adjacent to it, capillary locking nut (G2) with corresponding o-ring (G6), liquid feed shaft spacer (G4) and capillary o-rings (G5).....	20
Figure 3.7 Center body of the nozzle (C) with PTFE crown C1 for homogenization of the supporting flame flow and o-ring C2 (left). The sheath gas body (B) with the sheath gas homogenizer M and o-rings B1 and B2 is depicted on the right.....	21
Figure 3.8 Dispensing system (valve detail on the right).....	22
Figure 3.9 List of components filter.....	23
Figure 3.10 Vacuum pump and filter paper.....	24

Figure 3.11 Taking the filter paper from the filter.....	25
Figure 3.12 Stripping of powders from the filter paper.....	25
Figure 3.13 The nps10 viewing inside fume hood.....	26
Figure 3.12 (a) Step 1: Inserting the syringe into its holder with the piston, (b) fixing the terminal part of the piston by tightening the teflon stem, and (c) inserting the syringe fastener and fastening it finger-tight.....	26
Figure 4.1 DTA and TG curves of Mg based materials dried at 500oC for 2 hours in air.....	35
Figure 4.2 FTIR results of Mg based powders heat treated at different temperatures for 30 minutes in air.....	36
Figure 4.3 XRD pattern of MgO nanoparticles.....	37
Figure 4.4 XPS result of MgO nanoparticles showing 1s elemental scanning for oxygen.....	38
Figure 4.5 XPS result of MgO nanoparticles showing 1s elemental scanning for magnesium.....	38
Figure 4.6 XPS result of MgO nanoparticles showing general scanning for the magnesium oxide nanoparticles.....	39
Figure 4.7 SEM images of MgO nanoparticles ( a) 5.000X, (b) 10.000X and (c) 15.000X.....	40
Figure 4.8 Particle size distribution of MgO nanoparticle.....	41

## LIST OF TABLES

	<b>Page</b>
Table 3.1 Operating conditions of the NanoPowderNozzle.....	27
Table 4.1 The results of the turbidimeter .....	33
Table 4.2 XPS results of MgO particles showing elemental ID and quantification...39	

# CHAPTER ONE

## INTRODUCTION

### 1.1 General

The discovery of carbon nanotubes provided a new building block for the construction of molecular-scale circuits. Dekker's group demonstrated a carbon nanotube single-electron transistor operating at room temperature. In subsequent work, the same group constructed logic circuits with field-effect transistors based on single-wall carbon nanotubes, which exhibited power gain ( $> 10$ ) and large on-off ratios ( $>10^5$ ). A local-gate layout allowed for integration of multiple devices on a single chip; and one-, two-, and three-transistor circuits were demonstrated that exhibited digital logic operations, such as an inverter, a logic NOR, and a static random-access memory cell. In related work, Lieber's group has demonstrated logic circuits based on nanotube and semiconductor nanowires and Avouris' group built an inverter from chemically doped nanotubes on a silicon substrate (Goddard. et al., 2002).

In order to produce carbon nanotube, some catalyst materials such as iron (Fe), nickel (Ni), chromium (Cr), cobalt (Co) and magnesium oxide (MgO) are used in industrial applications. Of these catalyst materials, MgO is a versatile material according to its broad applications, such as in catalysis, hazardouswaste treatment and refractory materials (Yang & Lieber. 1996) (Huang & Li. 2005). The most conventional method for MgO synthesis is via the thermal decomposition of several magnesium salts (Alvarado. et al., 2000) (Ding. et al., 2001). Nevertheless, the resulting MgO particles inevitably possess relatively large and non-uniform particle sizes and low specific surface area, which are not preferable for the aforementioned applications.

Up to the present, extensive efforts have been devoted to the development of novel oxide materials with unique mesoporous structure (Kresge. et al., 1992). Nanostructured mesoporous MgO is also of research interest because of its diverse

properties, which originate from its structural characteristics (Wang, et al., 2007). Nanostructured mesoporous MgO is required to dope Fe, Ni, Cr and Co materials. Recently, there have been some methods for the synthesis of nanostructured mesoporous MgO, e.g., sol-gel, gel-templated technique (Jiu, et al., 2003), modified citrate precursor technique (Chen, et al. 2004), microwave plasma torch technique (Hong YC, Uhm HS. 2006), combustion technique (Nagappa & Chandrappa. 2007), high-temperature solid state synthesis, vapor-phase oxidation (Itatani, et al., 1997) and flame spray pyrolysis (Chen , et al., 2004).

Flame spray pyrolysis used in this study is a promising technique for the synthesis of high purity nanosized materials with controlled size and crystallinity in a single step. It was systematically investigated using an external-mixing gas-assisted atomizer supported by six premixed methane–oxygen flamelets (Chen, et. al., 2004) (Hong, Uhm. 2006). Moreover at low oxidant flow rates the specific surface area increased with increasing oxidant flow rate as the spray flame length was reduced leading to shorter residence time allowing less time for particle growth. Using oxygen as oxidant the droplets burn much faster than in air, thus product particles experience longer residence times at higher temperature causing lower specific surface area. Therefore the specific surface area of the nanocomposites can be controlled by adjusting the oxidant flow rates. After evaporation and combustion of precursor droplets, nanocomposites were formed by nucleation, condensation, coagulation and coalescence.

## **1.2 Organization of the Thesis**

In this study, we produced pure MgO nanoparticles using flame spray pyrolysis technique for application of carbon nanotube fabrication. After fabrication of nanosized MgO powders, they were characterized by using FT-IR, XRD, XPS, DTA-TG and SEM machines. It was found that the pure MgO nanoparticles was successfully produced for application of carbon nanotube fabrication.

With this context, chapters can be explained in details. Chapter one provides a brief introduction to the area of research and the research objectives of this thesis. In Chapter two, a comprehensive literature reviews concerning nanotechnology, carbon nanotube, properties and production of MgO nanoparticles in details. Chapter three, the experimental procedures of MgO nanoparticles are explained. Besides, the performed fire tests and characterizations are explained in this chapter. In Chapter four, the results concerning properties of MgO nanoparticles for application of carbon nanotube fabrication are demonstrated and discussed in details. Characterization of MgO nanoparticles is also analyzed in the same chapter. The conclusion and future plans are summarized in Chapter five.

## CHAPTER TWO

### THEORETICAL BACKGROUND

#### 2.1 Nanotechnology

The prefix *nano* in the word *nanotechnology* means a billionth ( $1 \times 10^{-9}$ ). Nanotechnology deals with various structures of matter having dimensions of the order of a billionth of a meter. While the word *nanotechnology* is relatively new, the existence of functional devices and structures of nanometer dimensions is not new, and in fact such structures have existed on Earth as long as life itself. The abalone, a mollusk, constructs very strong shells having iridescent inner surfaces by organizing calcium carbonate into strong nanostructured bricks held together by a glue made of a carbohydrate-protein mix. Cracks initiated on the outside are unable to move through the shell because of the nanostructured bricks. The shells represent a natural demonstration that a structure fabricated from nanoparticles can be much stronger.

The potential importance of clusters was recognized by the Irish-born chemist Robert Boyle in his *Sceptical Chymist* published in 1661. In it Boyle criticizes Aristotle's belief that matter is composed of four elements: earth, fire, water, and air. Instead, he suggests that tiny particles of matter combine in various ways to form what he calls corpuscles. He refers to "minute masses or clusters that were not easily dissipable into such particles that composed them" (Kwok, Ellenbogen. 2002).

It is not clear when humans first began to take advantage of nanosized materials. It is known that in the fourth-century A.D. Roman glassmakers were fabricating glasses containing nanosized metals. An artifact from this period called the Lycurgus cup resides in the British Museum in London. The cup is made from soda lime glass containing silver and gold nanoparticles. The color of the cup changes from green to a deep red when a light source is placed inside it. The great varieties of beautiful colors of the windows of medieval cathedrals are due to the presence of metal nanoparticles in the glass (Novoselov, et. al., 2004).

Richard Feynman was awarded the Nobel Prize in physics in 1965 for his contributions to quantum electrodynamics, a subject far removed from nanotechnology. Feynman was also a very gifted and flamboyant teacher and lecturer on science, and is regarded as one of the great theoretical physicists of his time. He had a wide range of interests beyond science from playing bongo drums to attempting to interpret Mayan hieroglyphics. The range of his interests and it can be appreciated by reading his lighthearted autobiographical book *Surely You're Joking, Mr. Feynman*. In 1960 he presented a visionary and prophetic lecture at a meeting of the American Physical Society, entitled "There is Plenty of Room at the Bottom," where he speculated on the possibility and potential of nanosized materials. He envisioned etching lines a few atoms wide with beams of electrons, effectively predicting the existence of electron-beam lithography, which is used today to make silicon chips. He proposed manipulating individual atoms to make new small structures having very different properties (Zhang, et. al., 2005).

Although Feynman presented his visionary lecture in 1960, there was experimental activity in the 1950s and 1960s on small metal particles. It was not called nanotechnology at that time, and there was not much of it. Uhlir reported the first observation of porous silicon in 1956, but it was not until 1990 when room-temperature fluorescence was observed in this material that interest grew. Other work in this era involved making alkali metal nanoparticles by vaporizing sodium or potassium metal and then condensing them on cooler materials called substrates. Magnetic fluids called ferrofluids were developed in the 1960s. They consist of nanosized magnetic particles dispersed in liquids. The particles were made by ball milling in the presence of a surface-active agent (surfactant) and liquid carrier (Kirk, et. al., 1981).

It was not until the 1980s with the emergence of appropriate methods of fabrication of nanostructures that a notable increase in research activity occurred, and a number of significant developments resulted. In 1981, a method was developed to make metal clusters using a high-powered focused laser to vaporize metals into a hot plasma. A gust of helium cools the vapor, condensing the metal atoms into clusters



of various sizes. In 1985, this method was used to synthesize the fullerene ( $C_{60}$ ) (Venkateswara, Sunandana. 2007).

The first observation was that materials have been and can be nanostructured for new properties and novel performance. The underlying basis for this is that every property of a material has a characteristic or critical length associated with it. For example, the resistance of a material that results from the conduction electrons being scattered out of the direction of flow by collisions with vibrating atoms and impurities, can be characterized by a length called the *scattering length*. This length is the average distance an electron travels before being deflected. The fundamental physics and chemistry changes when the dimensions of a solid become comparable to one or more of these characteristic lengths, many of which are in the nanometer range. One of the most important examples of this is what happens when the size of a semiconducting material is in the order of the wavelength of the electrons or holes that carry current. The electronic structure of the system completely changes. This is the basis of the quantum dot, which is a relatively mature application of nanotechnology resulting in the quantum-dot laser presently used to read compact disks (CDs). The electron structure is strongly influenced by the number of dimensions that are nanosized (Venkateswara, Sunandana. 2007) (Maedler, et. al., 2002).

The second general observation of the U.S. government study was a recognition of the broad range of disciplines that are contributing to developments in the field. Work in nanotechnology can be found in university departments of physics, chemistry, and environmental science, as well as electrical, mechanical, and chemical engineering. The interdisciplinary nature of the field makes it somewhat difficult for researchers in one field to understand and draw on developments in another area. As Feynman correctly pointed out, biological systems have been making nanometer functional devices since the beginning of life, and there is much to learn from biology about how to build nanostructured devices. How, then, can a solid-state physicist who is involved in building nanostructures but who does not know the difference between an amino acid and a protein learn from biological

systems? In order to accomplish this, it is necessary to include in each chapter some introductory material. Thus, the chapter on the effect of nanostructuring on ferromagnetism starts with a brief introduction to the theory and properties of ferromagnets (Uchida, et al. 1999) (Takato, et al.1988).

## 2.2 Carbon Nanotube

In nanotechnology, the more interesting nanostructures with large application potential are carbon nanotubes. One can think of a carbon nanotube as a sheet of graphite rolled into a tube with bonds at the end of the sheet forming the bonds that close the tube. Figure 2.1 shows the structure of a tube formed by rolling the graphite sheet about an axis parallel to C—C bonds. A single-walled nanotube can have a diameter of 2 nm and a length of 100 microns, making it effectively a one dimensional structure called a nanowire.

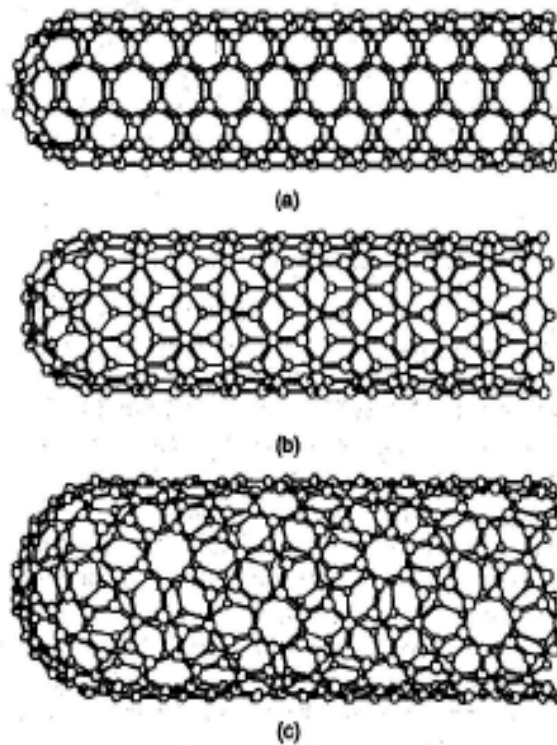


Figure 2.1 Illustration of some possible structures of carbon nanotubes, depending on how graphite sheets are rolled: (a) armchair structure; (b) zigzag structure; (c) chiral (Park, et. al., 2006).

Carbon nanotubes can be made by laser evaporation, carbon arc methods, and chemical vapor deposition. Figure 2.2 illustrates the apparatus for making carbon nanotubes by laser evaporation. A quartz tube containing argon gas and a graphite target are heated to 1200°C. Contained in the tube, but somewhat outside the furnace, is a water-cooled copper collector. The graphite target contains small amounts of cobalt and nickel that act as catalytic nucleation sites for the formation of the tubes. An intense pulsed laser beam is incident on the target, evaporating carbon from the graphite. The argon then sweeps the carbon atoms from the high-temperature zone to the colder copper collector on which they condense into nanotubes. Tubes 10-20 nm in diameter and 100 microns long can be made by this method.

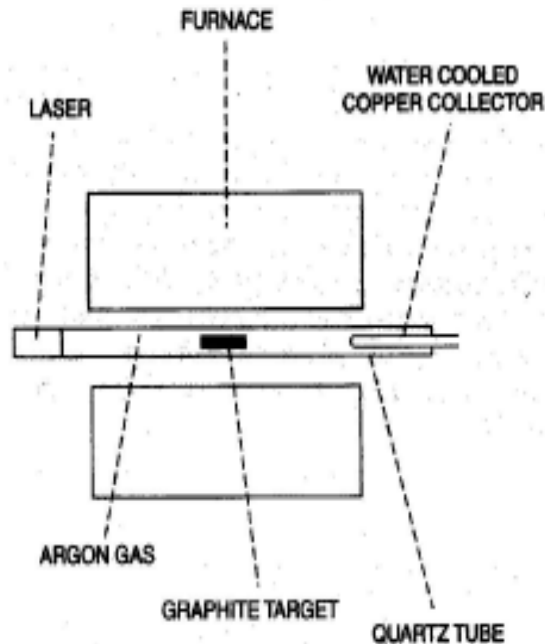


Figure 2.2 Experimental arrangement for synthesizing carbon nanotubes by laser evaporation (McKenna, et al., 2010).

The chemical vapor deposition method involves decomposing a hydrocarbon gas such as methane at 1100°C. As the gas decomposes, carbon atoms are produced that then condense on a cooler substrate that may contain various catalysts such as iron. This method produced tubes with open ends, which does not occur when other methods are used. This procedure allows continuous fabrication, and may be the

most favorable method for scale up and production. The mechanism of nanotube growth is not understood. Since the metal catalyst is necessary for the growth of single wall nanotubes, the mechanism must involve the role of the Co or Ni atoms. One proposal referred to as the "scooter mechanism" suggests that atoms of the metal catalyst attach to the dangling bonds at the open end of the tubes, and that these atoms scoot around the rim of the tube, absorbing carbon atoms as they arrive.

Generally when nanotubes are synthesized, the result is a mix of different kinds, some metallic and some semiconducting. A group at IBM has developed a method to separate the semiconducting from the metallic nanotubes. The separation was accomplished by depositing bundles of nanotubes, some of which are metallic and some semiconducting on a silicon wafer. Metal electrodes were then deposited over the bundle. Using the silicon wafer as an electrode, a small bias voltage was applied that prevents the semiconducting tubes from conducting, effectively making them insulators. A high voltage is then applied across the metal electrodes, thereby sending a high current through the metallic tubes but not the insulating tubes. This causes the metallic tubes to vaporize, leaving behind only the semiconducting tubes (Goddard, et. al., 2002).

### **2.3 Nanoparticle Production**

Nanostructured materials, nanocrystals, or nanophase materials are polycrystals with an ultra-fine grain size in the range of 3 to 100 nm. First results on the preparation of nanostructural materials by a compaction of nanometer-sized metal powders and their properties were reported by Russian investigators. However, the idea of a significant modification of the properties of materials by the formation of a nanocrystalline structure was first formulated by Gleiter and co-workers. After these publications nanocrystals have gained much interest of materials scientists, because they exhibit a number of improved properties as compared with otherwise the same polycrystals with conventional coarse-grain sizes. The spectrum of properties affected by the nanocrystalline structure ranges from the electronic ones to the

macroscopic mechanical behavior. A number of physical and mechanical properties of nanostructural materials have been found to be superior to the properties of conventionally coarse-grained polycrystals and are attractive for engineering applications. The ability of nanocrystalline alloys to deform superplastically at lower temperatures and higher strain rates is expected to significantly lower the costs of metal-forming technologies. High strength, ductility, and wear resistance can make the use of nanocrystalline refractory metals and ceramics as parts of high-temperature devices such as engines. Enhanced soft magnetic properties of nanocrystalline alloys, such as the low coercivity and high magnetic permeability, are already in use in transformers. The nanostructural materials have many orders of magnitude higher diffusion coefficient that can find applications, for example, in hydrogen storage technologies (Morokhov, et al. 1977) (Gleiter, 1981 and 1989)

There are several methods to production nanoparticles. They are chemical method, RF plasma, thermolysis and pulse laser methods.

Probably the most useful methods of synthesis in terms of their potential to be scaled up are chemical methods. There are a number of different chemical methods that can be used to make nanoparticles of metals. Several types of reducing agents can be used to produce nanoparticles such as NaBEt<sub>3</sub>H, LiBEt<sub>3</sub>H, and NaBH<sub>4</sub> where Et denotes the ethyl (.C<sub>2</sub>H<sub>5</sub>) radical. For instance, nanoparticles of molybdenum (Mo) can be reduced in toluene solution with NaBEt<sub>3</sub>H at room temperature, providing a high yield of Mo nanoparticles having dimensions of 1-5 nm. The equation for the reaction is



Nanoparticles of aluminum have been made by decomposing Me<sub>2</sub>EtNAlH<sub>3</sub> in toluene and heating the solution to 105°C for 2 hours (Me is methyl, CH<sub>3</sub>) (Parekh, et al., 2013).

As for RF plasma, the metal is heated above its evaporation point using high voltage RF coils wrapped around the evacuated system in the vicinity of the pestle. Helium gas is then allowed to enter the system, forming a high temperature plasma in the region of the coils. The metal vapor nucleates on the He gas atoms and diffuses up to a colder collector rod where nanoparticles are formed. The particles are generally passivated by the introduction of some gas such as oxygen. In the case of aluminum nanoparticles the oxygen forms a layer of aluminum oxide about the particle (Parekh, et al., 2013).

In thermolysis process, nanoparticles can be made by decomposing solids at high temperature having metal cations, and molecular anions or metal organic compounds. For example, small lithium particles can be made by decomposing lithium azide,  $\text{LiN}_3$ . The material is placed in an evacuated quartz tube and heated to  $400^\circ\text{C}$  in the apparatus (Parekh, et al., 2013).

Pulsed lasers have been used in the synthesis of nanoparticles of silver. Silver nitrate solution and a reducing agent are flowed through a blender like device. In the blender there is a solid disk, which rotates in the solution. The solid disk is subjected to pulses from a laser beam creating hot spots on the surface of the disk. Silver nitrate and the reducing agent react at these hot spots, resulting in the formation of small silver particles, which can be separated from the solution using a centrifuge. The size of the particles is controlled by the energy of the laser and the rotation speed of the disk. This method is capable of a high rate of production of 2-3 g/min (Parekh, et al., 2013).

## **2.4 Magnesium Oxide**

$\text{MgO}$ , or magnesia, is a white hygroscopic solid mineral that occurs naturally as periclase and is a source of magnesium. It has an empirical formula of  $\text{MgO}$  and consists of a lattice of  $\text{Mg}^{2+}$  ions and  $\text{O}_2^-$  ions held together by ionic bonds. Magnesium hydroxide forms in the presence of water ( $\text{MgO} + \text{H}_2\text{O} \rightarrow \text{Mg}(\text{OH})_2$ ), but it can be reversed by heating it to separate moisture.

A refractory material is one that is physically and chemically stable at high temperatures. "By far the largest consumer of magnesia worldwide is the refractory industry, which consumed about 56% of the magnesia in the United States in 2004, the remaining 44% being used in agricultural, chemical, construction, environmental, and other industrial applications." (Mark,2006).

MgO is one of the raw materials for making Portland cement in dry process plants. If too much MgO is added, the cement may become expansive. Production of MgO-based cement using serpentinite and waste CO<sub>2</sub> (as opposed to conventional CaO-based cement using fossil fuels) may reduce anthropogenic emissions of CO<sub>2</sub> (McKenna, 2010). Furthermore, MgO is a relatively poor desiccant, but because it neutralizes sulfur oxide acids created by oxidation of Kraft-processed papers, it is used by many libraries for preserving books (Ferro, et al., 2012).

In medicine, magnesium oxide is used for relief of heartburn and sore stomach, as an antacid, magnesium supplement, and as a short-term laxative. It is also used to improve symptoms of indigestion. Side effects of magnesium oxide may include nausea and cramping (Magnesium Oxide. MedlinePlus. Last reviewed 02/01/2009). In quantities sufficient to obtain a laxative effect, side effects of long-term use include enteroliths resulting in bowel obstruction (Tatekawa, et al. 1996).

MgO is used as an insulator in industrial cables, as a basic refractory material for crucibles and as a principal fireproofing ingredient in construction materials. As a construction material, magnesium oxide wallboards have several attractive characteristics: fire resistance, moisture resistance, mold and mildew resistance, and strength.

It is used as a reference white color in colorimetry, owing to its good diffusing and reflectivity properties (Tellex, et al., 1955). It may be smoked onto the surface of an opaque material to form an integrating sphere. It is used extensively in heating as a component of "CalRod"-style heating elements. There are several mesh sizes available and most commonly used ones are 40 and 80 mesh per the American

Foundry Society. The extensive use is due to its high dielectric strength and average thermal conductivity. MgO is usually crushed and compacted with minimal airgaps or voids. The electrical heating industry also experimented with aluminium oxide, but it is not used anymore (Tellex, et al., 1955).

MgO is one of the most promising solid base material having catalytic applications. A novel, simple, efficient, inexpensive, additives free and green synthesis protocol for magnesium oxide nano-particles using concentrated solar energy has been reported. Solar energy being a greener source of energy differs from conventional heating systems. Although, the sunlight associated with the photochemical conversion is not excluded completely, the solar energy used in heating process might provide thermodynamic route to form stable MgO nanoparticles. The concept of concentrated solar energy is advantageous in the synthesis of nanomaterials due to the dual energy effect (radiation and thermal). The flux of solar radiations along with developed thermal energy speed up the reaction. Solar energy heating offers the advantages like rapid heat transfer, volumetric and selective heating, avoiding of sophisticated equipment and pollution free route as there are no combustion products. This synthetic protocol is much simpler than previous reports, avoiding complex and multistep reaction schemes, additives, conventional energy source and expensive equipments (Parekh, et al., 2013).

Metal oxides are of immense interest to the scientists due to their enhanced surface chemistry and high surface area. MgO is one of the most significant metal oxides having variety of applications in catalysis, refractory material industries, paint and superconductors. The synthesis of nanomaterials can be achieved using template-assisted, vapour-liquid-solid, colloidal micellar, sol-gel method, and microwave based methods. Conventionally, MgO nanoparticles are synthesized via thermal decomposition of various magnesium salts. However, the aforesaid methodologies are not preferable due to the harsh reaction conditions, the use of toxic reagents, high pressure, specialized equipment setup and the use of conventional non-renewable energy sources. Thus, the synthesis of MgO nanoparticles by green and inexpensive



method with its catalytic application is a subject of current work (Parekh, et al., 2013).

Magnesium (Mg) is a moderately reactive alkaline earth metal. (The Alkaline Earth's comprise Group 2A of the periodic table of the elements. They are referred to as alkaline because their oxides are basic in water. The term "Earth" was used by early alchemists to describe nonmetals, the oxides in this case, that did not melt in their furnaces.) At room temperature, Mg reacts only very slowly with oxygen and can be kept for long periods of time without appreciable oxide build-up. At elevated temperatures, however, Mg will ignite in an excess of oxygen gas, burning with an intensely white flame and producing MgO. Because of the brightness of its flame, Mg is used in flares and in photographic flashbulbs (General Chemistry Laboratory., 2013).

## **2.5 Sol–Gel Synthesis of MgO Nanocrystallites**

For synthesis of MgO nano-crystallites, magnesium nitrate hexahydrate  $[\text{Mg}(\text{NO}_3)_2 \cdot 6\text{H}_2\text{O}]$  and oxalic acid  $[(\text{COOH})_2 \cdot 2\text{H}_2\text{O}]$  precursors in 1:1 molar ratio are first dissolved separately in ethanol and filtered to obtain two clear solutions. These are then mixed to yield a thick white gel which, in turn, is digested for 12 hours and dried at 100 °C for 24 hours, ground, sieved through 240 mesh to get fine powder of magnesium oxalate dihydrate ( $\alpha\text{-MgC}_2\text{O}_4 \cdot 2\text{H}_2\text{O}$ ). Finally, the oxalate is decomposed at 500, 600, 800, and 1000 °C for 2 hours each in air, oxygen, or nitrogen ambient to yield MgO. The stoichiometry of  $\text{MgO}_{1-x}$  obtained by pyrolysis of anhydrous magnesium oxalate in vacuum at 350–500 °C is known to vary up to a maximum of  $x=0.01$  due to release of excess  $\text{CO}_2$  and less CO than given by the reaction  $\text{MgC}_2\text{O}_4 \rightarrow \text{MgO} + \text{CO}_2 + \text{CO}$  (Ehre, et al., 2005). Some deviation in stoichiometry from MgO is therefore expected here as well depending upon the temperature and environment chosen for the decomposition process. Also, the deviation is expected to be substantial in nitrogen and minimal in oxygen (Ashok, et al., 2011).

## 2.6 Flame Spray Pyrolysis Method

Flame spray pyrolysis is a high temperature flame process primarily for synthesis of metal-oxide nanoparticles from organometallic or metal-salt precursors. Therefore, the liquid or solid precursor is dissolved in or diluted with an appropriate organic solvent and sprayed with a two-phase nozzle into a methane or hydrogen/oxygen flame. Thereby, the resulting droplets of dissolved precursor are combusted and lead to clusters of the product material. In the high temperature environment of the flame, these clusters grow to product nanoparticles by collision and sintering and/or surface growth processes. Product particles must be recovered from the off-gas with a collection device such as a filter.

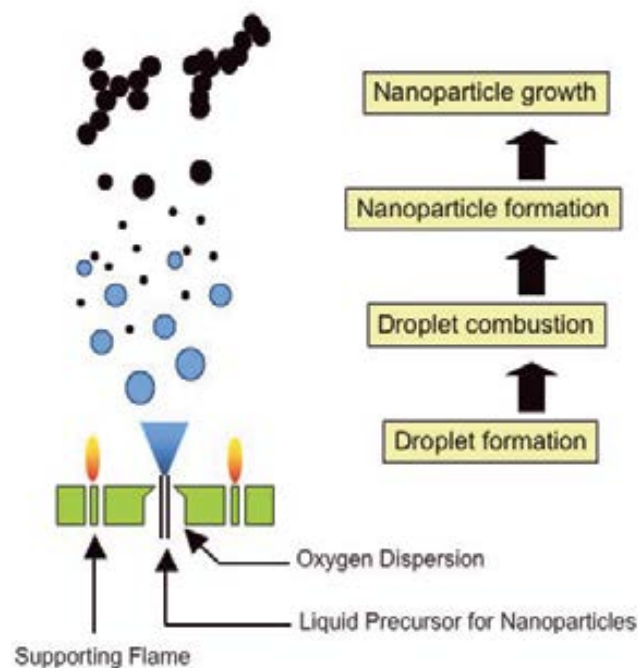


Figure 2.3 Schematic representation of the flame spray pyrolysis process (Maedler, et al., 2002)

Due to the high temperature environment of the flame (up to 2500°C, depending on raw materials and flame conditions), product nanoparticles are typically fully oxidized and crystalline. Thus, post-synthesis heat treatment steps are typically not required and the nanopowders can directly be used for further processing. Product

particle properties like size, agglomeration and to a certain extent shape can be influenced by the flame conditions and precursor composition.

Multi-component or doped nanoparticles can be made by mixing different precursors before feeding them into the spray nozzle. As particle synthesis is based on a high-temperature oxidation process in a flame, the range of product materials is mainly limited to single or multi-component oxide ceramics. However, also other oxygen-containing compounds like phosphates or carbonates as well as noble metal nanoparticles can be produced in the appropriate flame environment (Mädler, et al., 2002) (Strobel , Pratsinis. 2007).

## **CHAPTER THREE**

### **EXPERIMENTAL METHOD**

#### **3.1 Objective**

The objective of this thesis is synthesis and characterization of MgO nanoparticles using flame spray pyrolysis for carbon nanotube production. After the synthesis of MgO nanoparticles, they were characterized by using DTA-TG, FT-IR, XRD, XPS, SEM and particle size analyzer machines.

#### **3.2 Materials**

In this study, magnesium ethoxide ( $C_4H_{10}MgO_2$ ) with 114,43 g/mole of molecular weight was used to produce MgO nanoparticles as a precursor. 70 mL of methanol was utilized to dissolve magnesium ethoxide powders as a solvent. 1 mL of acetic acid was used as a chelating agent.

#### **3.3 Production Technique**

In order to produce MgO nanoparticles, flame spray pyrolysis was used for this purpose. In this technique, lab-scale systems are useful for the production of nanomaterials in the form of powders such as simple oxides, complex oxides, composites, and noble metals. This system has nozzle unit, nanopowders nozzle and filters. In nozzle unit & nanopowders nozzle can be seen in Figure 3.1. The nozzle unit is the main part of the system, where a water-cooled spray nozzle (nanopowder nozzle) is integrated in the flame spray pyrolysis system or nano powder synthesizer (Model Tethis nps 10) and connected to a pre-installed system of liquid and gas supplies. It is a two-phase nozzle with a replaceable capillary through which a precursor solution is delivered and dispersed by a co-flowing stream of oxygen. A supporting flame, which is ignited by an automated spark-ignition lance, guarantees the combustion of the precursor spray and prevents it from extinguishing. The gas connections are on the back left side of the nps 10. Stainless steel tubes carry the

gases to four mass flow controllers, which deliver dispersion oxygen, supporting flame methane and oxygen as well as an optional sheath gas to the spray nozzle. The flame spray nozzle is water-cooled to avoid heat-up: the cooling water connections are on the back of the system on the right. Flow meters controlling the cooling water flow to the spray nozzle are already integrated into the nps 10. External flow meters do not have to be used (Figures 3.2-3.6).



Figure 3.1 Nozzle unit and nanopowders nozzle inside flame spray pyrolysis device



Figure 3.2 Gas and water connections to the nozzle on the Nozzle Unit internal wall: 1–nozzle cooling water outlet; 2–nozzle cooling water inlet; 3–premixed supporting flame gas; 4–dispersion oxygen; 5–sheath gas (optional); 6–capillary cooling water outlet; 7–capillary cooling water inlet

In this system, component identification table for the nano powder nozzle can be seen in Figure 3.3 including A: Mounting plate, B: Sheath gas body, B1: Upper sheath gas body o-ring, B2: Lower sheath gas body o-ring, C: Center body with gas inlets (capillary cooling circuit), C1: Supporting flame flow homogenizer, C2: Center body o-ring, D: Connector for dispersion gas, E: Luer Lock connector of liquid feed capillary, F: Connector for premixed supporting flame gas, G: Liquid feed shaft

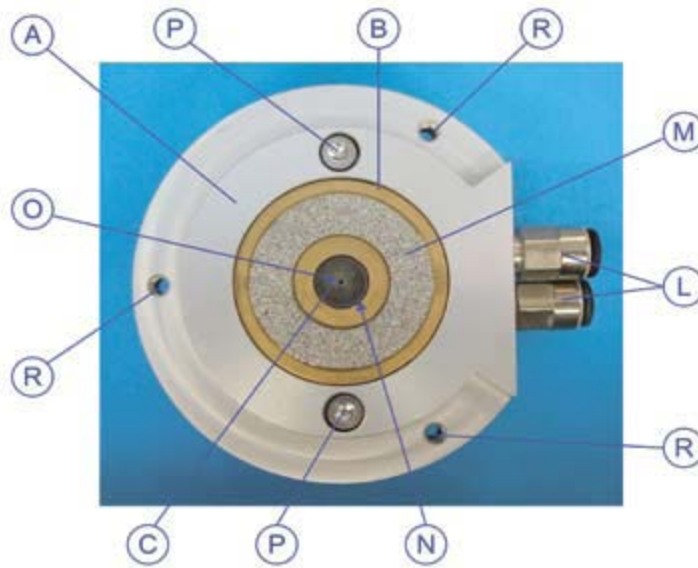


Figure 3.3 Top view of the NanoPowderNozzle with capillary and dispersion gas outlet (O), the concentric outlet gap for the premixed supporting flame gas (N) and sintered metal ring for the optional sheath gas flow (M)

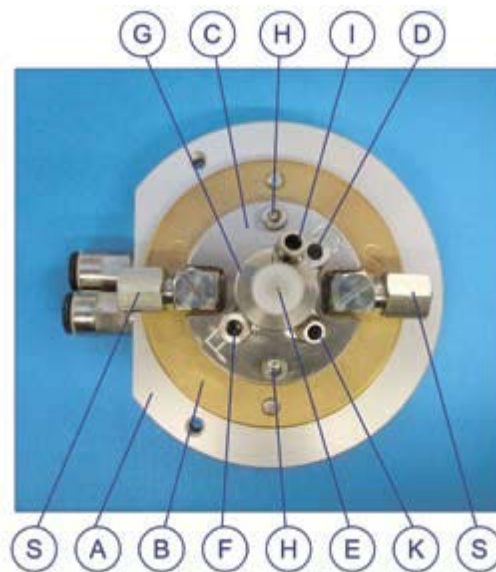


Figure 3.4 View of the back-side of the nano powder nozzle with connectors for the liquid feed (E), dispersion gas (D), premixed supporting flame gas (F), optional sheath gas (S), and capillary cooling water (I, K)

(capillary cooling circuit), G1: Dispersion pressure regulator (capillary cooling circuit), G2: Capillary locking nut (capillary cooling circuit), G3: Upper and lower liquid feed shaft o-ring, G4: Liquid feed shaft spacer, G5: Upper and lower capillary o-ring, G6: Capillary locking nut o-ring, H: Screws for center body attachment, I:

Connector for capillary cooling water inlet, K: Connector for capillary cooling water outlet, L: Connectors for nozzle cooling water inlet and outlet, M: Sheath gas homogenizer, N: Outlet gap for premixed supporting flame gas, O: Capillary for liquid feed (with surrounding dispersion gas gap), P: Screws fixing the nozzle to the mounting plate, R: Bores for nozzle mounting and S: Connectors for sheath gas.



Figure 3.5 Liquid feed shaft, consisting of the dispersion pressure regulator (G1), locking nut (G2) and liquid feed shaft o-rings (G3)

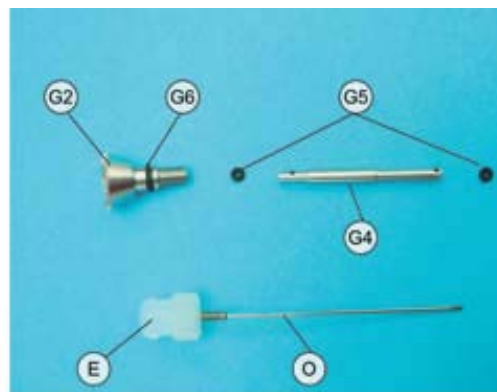


Figure 3.6 Liquid feed shaft inner components necessary for the capillary cooling circuit: liquid feed capillary (O) with Luer Lock connector (E) and M2 thread adjacent to it, capillary locking nut (G2) with corresponding o-ring (G6), liquid feed shaft spacer (G4) and capillary o-rings (G5)

The assembled nano powder nozzle is depicted in Figures 3.3 and 3.4. The top view (Figure 3.3) shows the nozzle mounting plate A made from anodized aluminum into which the nozzle is inserted and fixed with screws P. Bores R allow the attachment of the nano powder nozzle to its holder in the nps10 nozzle unit. Between

the sheath gas body B made out of brass and the mounting plate A are o-ring sealed channels for the nozzle cooling water (see Figure 3.7).

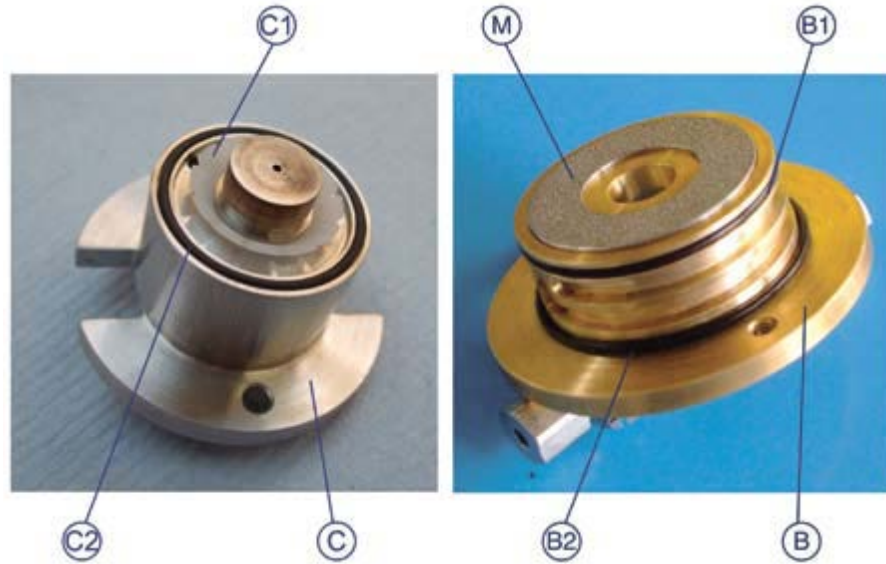


Figure 3.7 Center body of the nozzle (C) with PTFE crown C1 for homogenization of the supporting flame flow and o-ring C2 (left). The sheath gas body (B) with the sheath gas homogenizer M and o-rings B1 and B2 is depicted on the right

The channels are connected to a cooling water line through the nozzle cooling water inlet and outlet connectors L (Legris connectors for 6 mm o.d. flexible tubes). The sheath gas body B holds the sheath gas homogenizer M, a porous sintered stainless steel plate with a pore size of approx. 50  $\mu\text{m}$  through which a uniform sheath gas flow can be established. Operation of the nano powder nozzle with sheath gas is optional. A sheath gas must not be provided for nozzle functionality under the typical operating conditions.

The stainless steel center body C of the nano powder nozzle is inserted into the sheath gas body B and fixed with screws H (Figure 3.5). Thereby, a small gap N is formed on the upper side of the nozzle through which the premixed gases for the supporting flame exit. A bore through the center of the stainless steel center body C allows to introduce the liquid feed capillary O and to form a gap for the dispersion gas.



The back-side view in Figure 3.5 additionally shows the stainless steel liquid feed shaft G which holds the capillary O. G has an integrated gap for capillary cooling water (see Figure 3.3) which is introduced through the Legris connector I and exits through Legris connector K. Connectors I and K are for flexible tubes with 3 mm outer diameter.

The nano powder synthesizer is equipped with a high-precision low-pulsation syringe pump that meters the precursor solution to the flame spray nozzle. The syringe can be filled with precursor or solvent for cleaning from standard laboratory flasks connected through a 3-way valve and facilitating product change (Figure 3.8).

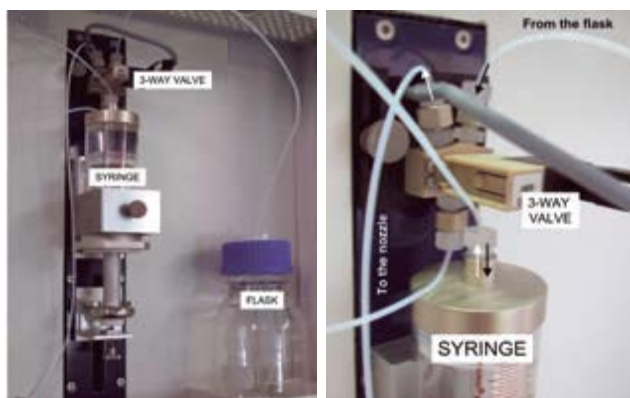


Figure 3.8 Dispensing system (valve detail on the right)

In this system, there are filters which contain A: Cylindrical stainless steel filter holder, B: Water-cooled aluminum/stainless steel lid, C: Closing knobs, D: Quick-connectors for the cooling water supply, E: DN 40 ISO-KF stainless steel crosspiece, F: DN 40 ISO-KF flexible stainless steel tube, 3m length, G: Vacuum pump (complete with inlet and outlet adapters and filter), H: Pressure gauge for vacuum line (analog) assembled on KF40 flange, I: Temperature sensor Pt-100 assembled on KF40 flange, J: Glass fiber filters (pack of 100) and K: Holes for installation. Figures 3.8-3.11 shows filters system and related equipments. Figure 3.12 depicts the nps10 viewing inside fume hood.

In preparation for operation of the system, first of all the flask filled with the desired liquid and position it in its tray were prepared. The syringe was prepared, as

shown in Figure 3.13. Here the syringe into its holder with the piston was inserted and the syringe was pointed up as a first step (Figure 3.13.a). The terminal part of the piston is fixed by tightening the teflon stem as a second step (Figure 3.13.b). the syringe fastener was inserted and it was fastened with finger-tight as a third step (Figure 3.13.c). After that, the right tube coming from the valve into the cap of the precursor flask was inserted, and the left tube to the liquid feed capillary of the nozzle was connected. The ventilation system of the fume hood was turned on the system, before the cooling water and the gas supplies were opened respectively. Consequently the following items were checked in the system. The nps10 was securely installed in the fume hood. No objects and especially no flammable gases, liquids and solids that are not needed for the operation of the nps10 were placed in the fume hood. The fume hood ventilation was functional and the hood can be closed

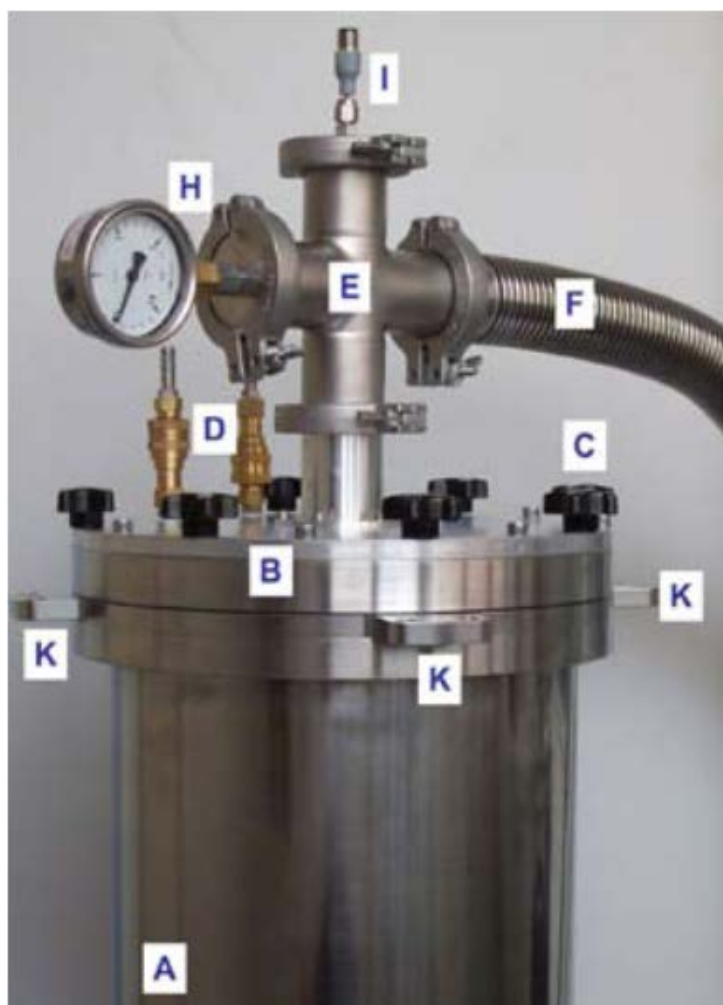


Figure 3.9 List of components filter



Figure 3.10 Vacuum pump and filter paper



Figure 3.11 Taking the filter paper from the filter



Figure 3.12 Stripping of powders from the filter paper

during operation to prevent off-gas from the nano powder nozzle to escape into the workplace and to prevent people from reaching into the fume hood. The nozzle was properly assembled and fixed in its holder. The cooling water circuit was properly connected and leak-free. If the liquid feed nozzle has been installed properly no cooling water should leak out of the liquid feed shaft neither at the dispersion gas gap around the outlet side of the liquid feed capillary nor at the capillary locking nut near the Luer Lock connector on the inlet side of the capillary. In case cooling water leaks out, tighten the capillary locking nut further. All gas lines were properly connected and leak-free. It should be make sure that the pressure in any of the gas lines does not exceed 10 bar. The liquid feed capillary was inserted and properly connected and was leak-free. The chemical compatibility of the substances to be used with the nano powder nozzle, the supply lines and the surrounding infrastructure was assured. The operators were aware of the reactions taking place when operating the nano powder nozzle, the reaction products and possible by-products formed, also in the case of an incomplete combustion.

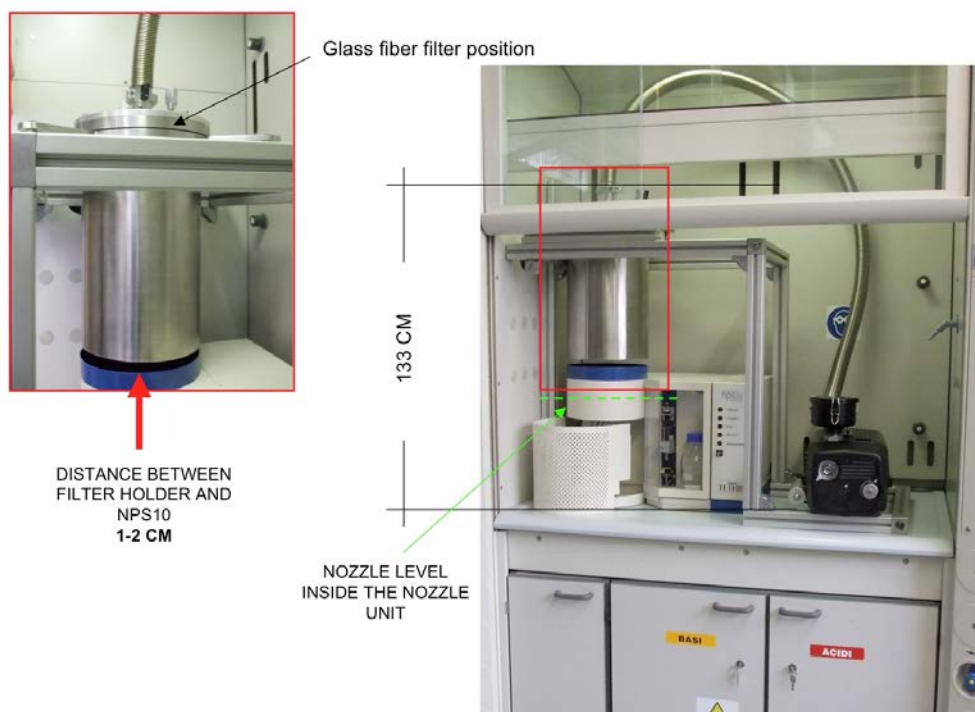


Figure 3.13 The nps10 viewing inside fume hood

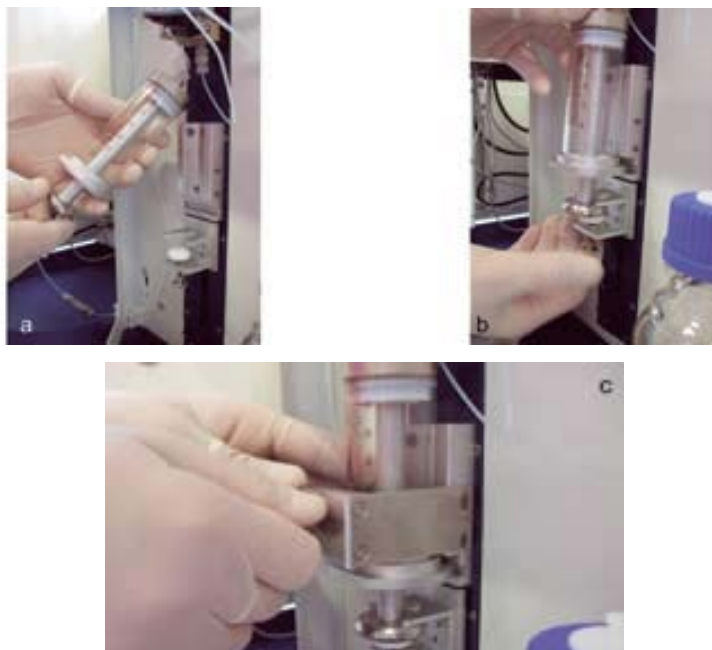


Figure 3.12 (a) Step 1: Inserting the syringe into its holder with the piston, (b) fixing the terminal part of the piston by tightening the teflon stem, and (c) inserting the syringe fastener and fastening it finger-tight

In start up procedure of the system, the NCS control software was started with a double click on the NCS icon. At the start-up, all the lights on the nps10 control unit front flash for a few seconds: the system is ready to operate when all the LEDs are off, except the last one “Advanced mode” that can be on, in case the user is operating in this mode. If a new syringe is used, set its parameters in the corresponding pop-up window, otherwise the software uses the parameter set that was used last. The syringe is calibrated, if needed. After the dispersion gas pressure drop is checked and calibrated, the syringe is filled by clicking on the “Fill” button. A pop up window appear, to set the filling speed and the syringe volume to fill. “Ignition” button is checked to start the flame. After 30 seconds the “Flame ON” yellow LED switches on. The gases and the precursor target flows are set in the main window (flame, dispersion and optional sheath gas), or choose a Recipe from the software menu. The flame Target Flow already has a default value at the ignition starting that can be changed, before the nanoparticle production begins. The “Start” buton is clicked to start the nanoparticle production. When the precursor in the syringe has been used up, the syringe can be refilled without shutting down the flame. To do this, the “Fill” buton is clicked: when the syringe is full, it is possible restart the production

(“Start”). In operating conditions, the nano powder nozzle with the operating conditions was summarized in Table 3.1.

Table 3.1 Operating conditions of the nano powder nozzle.

Parameters	Their values	
Oxygen dispersion gas	1.5 bar (g)	5 L/min
Methane for supporting flame	atm.	1.5 L/min
Oxygen for supporting flame	atm.	3 L/min
Liquid feed		5 mL/min
Capillary cooling water		100 mL/min
Nozzle cooling water		1 L/min

### 3.4 Solution Characterization

#### 3.4.1 Turbidimeter

Turbidimetry (the name being derived from turbidity) is the process of measuring the loss of intensity of transmitted light due to scattering effect particles suspended in it. Light is passed through a filter creating a light of known wavelength which is then passed through a cuvette containing a solution. A photoelectric cell collects the light which passes through the cuvette. A measurement is then given for the amount of absorbed light (Mary C. Haven, Gregory A. Tetrault, Jerald R. Schenken 1994).

Turbidity is the cloudiness or haziness of a fluid caused by individual particles (suspended solids) that are generally invisible to the naked eye, similar to smoke in air. The measurement of turbidity is a key test of water quality. Fluids can contain suspended solid matter consisting of particles of many different sizes. While some suspended material will be large enough and heavy enough to settle rapidly to the bottom of the container if a liquid sample is left to stand (the settleable solids), very small particles will settle only very slowly or not at all if the sample is regularly agitated or the particles are colloidal. These small solid particles cause the liquid to appear turbidity.

Turbidity (or haze) is also applied to transparent solids such as glass or plastic. In plastic production haze is defined as the percentage of light that is deflected more than  $2.5^\circ$  from the incoming light direction (Thermal laminating films from 29/09/2013). In this technique, turbidity of the prepared solutions was measured whether powder based precursor is dissolved very well.

### **3.4.2 pH Meter**

The pH meter measures the concentration of hydrogen ions ( $H^+$ ) in an aqueous solution that are responsible of its acidity or alkalinity. It is formed, in its simplest and most used version, by the so-called glass electrode, a tube made by a special semi-porous glass containing an HCl solution with a known and constant concentration (better named as activity) of  $H^+$  and a silver (Ag) probe covered by AgCl (silver chloride) immersed in it, to keep constant the  $H^+$  and  $Cl^-$  activities in this solution (Phmeter from, 2013).

Just few mm outside this glass tube, there's another Ag probe, equally immersed in the solution to be measured for its  $H^+$  activity and linked with another. Ag/AgCl glass electrode that is the reference, with a constant electric potential. This electrode is small, also few cm long, easy and fast to use and sensible ( $\pm 0.001$  pH units) and the relation between the potential measured and the  $H^+$  activity (a) is expressed by the Nernst Equation, very important in chemistry, where E is the electric potential (electrode/solution):

$$E = 0.059 \log [a_o(H^+) / a_1(H)] \quad (3.1)$$

where  $a_o(H^+)$  is the activity of  $H^+$  inside the electrode.

In this study, the pH of the Mg based solutions was measured using Mettler Toledo Inlab 412 pH meter of a glass electrode. After that, their acidic and basic characteristics were evaluated for further processing.

### **3.5 Material Characterization**

#### ***3.5.1. Differential Thermal Analysis-Thermogravimetry (DTA-TG)***

Thermal methods are based upon the measurement of the dynamic relationship between temperature and some property of the system such as mass and heat absorbed by or evolved from it. Differential Thermal Analysis (DTA) and Thermogravimetry (TG) are the most important thermal methods used in characterization of materials. In DTA the heat absorbed or emitted by a system is observed by measuring the temperature difference  $\Delta T$  between the sample and an inert reference material (generally alumina powder), as the temperature of both is increased at a constant rate. TG analysis is concerned with the change in weight of a material as its temperatures changes. Many series of thermal analysis techniques can be combined with other non-thermal technique for valuable multiple-parameter information as in our DTA/TG system. The thermal behaviours of Mg based xerogel were evaluated to observe decomposition and phase formation at a heating rate of 10°C/min in the temperature range of 25-1100 °C under air atmosphere by using DTA/TG machine (DTG-60H Shimadzu).

#### ***3.5.2 Fourier Transform Infrared Spectroscopy (FTIR)***

FTIR is a powerful tool for identifying types of chemical bonds in a molecule by producing an infrared absorption spectrum that is like a molecular "fingerprint". Each different material is a unique combination of atoms, so two different compounds never produce the exact same infrared spectrum. Therefore, infrared spectroscopy can result in qualitative analysis of every different kind of material. By interpreting the infrared absorption spectrum, the chemical bonds in a molecule can be determined. In principle, molecular bonds vibrate at various frequencies depending on the elements and the type of bonds. For any given bond, there are several specific frequencies at which it can vibrate. According to quantum mechanics, these frequencies correspond to the ground state (lowest frequency) and several excited states (higher frequencies). One way to cause the frequency of a molecular vibration



to increase is to excite the bond by having it absorb light energy. For any given transition between two states the light energy (determined by the wavelength) must exactly equal the difference in the energy between the two states. The energy corresponding to these transitions between molecular vibrational states is generally 1-10 kilocalories/mole which corresponds to the infrared portion of the electromagnetic spectrum. The results are generally plotted as a function transmittance or absorbance versus wavelength. The conversion between transmittance to absorbance data is:

$$A = \log (1/T) \quad (3.2)$$

where A is absorbance and T is transmittance. In addition to qualitative analysis, the size of the peaks in the spectrum is a direct indication of the amount of material present. With suitable software algorithms, infrared is also an excellent tool for quantitative analysis.

The infrared spectra of the samples were recorded with a Thermo Scientific S10 FT-IR instrument equipped with ATR apparatus in the spectra range between 4000 and 650  $\text{cm}^{-1}$  with a resolution of 4  $\text{cm}^{-1}$ . All of the samples were characterized by FTIR by which % transmittance as a function of wavelength and % absorbance as a function of wavenumber curves can be obtained.

### ***3.5.3 X-Ray Diffraction (XRD)***

X-ray crystallography is a method used for determining the atomic and molecular structure of a crystal, in which the crystalline atoms cause a beam of X-rays to diffract into many specific directions. By measuring the angles and intensities of these diffracted beams, a crystallographer can produce a three-dimensional picture of the density of electrons within the crystal. From this electron density, the mean positions of the atoms in the crystal can be determined, as well as their chemical bonds, their disorder and various other information (Kepler, 1611).

Since many materials can form crystals—such as salts, metals, minerals, semiconductors, as well as various inorganic, organic and biological molecules—X-ray crystallography has been fundamental in the development of many scientific fields. In its first decades of use, this method determined the size of atoms, the lengths and types of chemical bonds, and the atomic-scale differences among various materials, especially minerals and alloys. X-ray crystallography is still the chief method for characterizing the atomic structure of new materials and in discerning materials that appear similar by other experiments (Kepler, 1611) (Steno, 1669).

XRD is extensively used to investigate the structural properties of MgO powders produced by flame spray pyrolysis. All materials were analyzed by means of XRD with a grazing angle attachment and an incident angle of  $1^\circ$  (Thermo Scientific XRD). X-Ray radiation of  $\text{CuK}_\alpha$  was set at 40 kV and 36 mA with a scanning speed of  $2^\circ$   $2\theta/\text{min}$ , from  $15^\circ$  to  $80^\circ$ .

#### ***3.5.4 X-ray Photoelectron Spectroscopy (XPS)***

X-ray photoelectron spectroscopy (XPS) is a quantitative spectroscopic technique that measures the elemental composition, empirical formula, chemical state and electronic state of the elements that exist within a material. XPS spectra are obtained by irradiating a material with a beam of X-rays while simultaneously measuring the kinetic energy and number of electrons that escape from the top 1 to 10 nm of the material being analyzed. XPS requires ultra-high vacuum (UHV) conditions. It can be also used to analyze the surface chemistry of a material in its "as received" state, or after some treatment, for example: fracturing, cutting or scraping in air or UHV to expose the bulk chemistry, ion beam etching to clean off some of the surface contamination, exposure to heat to study the changes due to heating, exposure to reactive gases or solutions, exposure to ion beam implant, exposure to ultraviolet light.

XPS detects all elements with an atomic number ( $Z$ ) of 3 (lithium) and above. It cannot detect hydrogen and helium, because the diameter of these orbitals is so small, reducing the catch probability to almost zero. It is routinely used to analyze all

solid materials (Crist, B.V., 2011). In this study, MgO nanoparticles were analyzed as elemental via XPS (Thermo-Scientific, Al-K $\alpha$ ). The device was calibrated according to gold 4f<sub>7/2</sub>. 10<sup>-8</sup> mbar under vacuum was studied and from a single point was done 20 scanning. Pass energy and energy step size were determined as 150 eV and 1 eV.

### ***3.5.5 Scanning Electron Microscopy (SEM)***

A scanning electron microscope (SEM) is a type of electron microscope that produces images of a sample by scanning it with a focused beam of electrons. The electrons interact with electrons in the sample, producing various signals that can be detected and that contain information about the sample's surface topography and composition. The electron beam is generally scanned in a raster scan pattern, and the beam's position is combined with the detected signal to produce an image. SEM can achieve resolution better than 1 nanometer. Specimens can be observed in high vacuum, low vacuum and in environmental SEM specimens can be observed in wet conditions (McMullan, 1988 & 2006) In this study, the surfaces of MgO nanoparticles were examined by using Coxem em30 MiniSEM instrument operating at an accelerating voltage of 5-10 kV. Surfaces were coated with gold to be conductive.

### ***3.5.6 Particle Size Analysis***

After flame spray pyrolysis, the particle size distribution of MgO nanoparticles was determined using particle size analyzer which uses light scattering techniques to measure hydrodynamic size of nanoparticles. The particle size distribution was measured using Malvern Zeta Sizer Nano ZS90 (EMUM, DEU). Water was used as a dispersant and the temperature was set to 25°C.

## CHAPTER FOUR

### RESULTS AND DISCUSSION

#### 4.1. Solution Characteristics

Prior to powder production process, Mg based solutions were characterized with the aid of turbidimeter and pH meter.

##### 4.1.1 Turbidity

With turbidity experiments, whether magnesium ethoxide precursor materials are dissolved very well in solutions is understood by looking ntu values before process. As stated before, the turbidity values of the solutions vary in the range of 0 ntu and 1,000 ntu. It is interpreted that powder based precursors are completely dissolved as turbidity value approaches to 0 ntu and they are not dissolved and some powder particles are suspended in a solution as it approaches to 1000 ntu. In this experiment, turbidity value of the solutions was measured as 4.42 ntu. Table 4.1 shows turbidity results of the prepared solutions. Based on the turbidity value, it can be pointed that Mg based powder is completely dissolved in the solutions.

Table 4.1 The results of the turbidimeter

Number of Measurement	Measurements
1	5.01
2	4.25
3	4.21
4	4.22
Average	4.42

#### ***4.1.2 Acidic/Basic Characteristics***

The pH measurement refers to determination of the activity of hydrogen ions in Mg based based solution. Many important properties of the solution can be determined from an accurate measurement of pH, including the acidity of a solution and the extent of a reaction in the solution. Many chemical processes and properties, such as the speed of a reaction and the solubility of a compound, can also depend greatly on the pH of the solution. The pH value of the obtained solution was determined as 6.26 at 39.4°C in air. Therefore it was found that the prepared solutions is nearly acidic.

#### **4.2 Material Characteristics**

After powder production process, MgO nanoparticles were characterized through DTA-TG, FTIR, XRD, SEM and particle size measurement machines and comparatively discussed with literature.

##### ***4.2.1 DTA-TG Analysis***

Now that exothermic and endothermic reactions are significant in flame spray pyrolysis, DTA-TG analysis are carried out to investigate Mg based xerogel which was dried at 500°C for 2 hours in air. DTA-TG analyses are performed by heating up at the rate of 10 °C/min at temperatures between 25°C and 1100°C in air. DTA analysis of Mg based xerogel is demonstrated in Figure 4.1, showing that there are three thermal reactions including solvent removal at approxiametly 100°C. This is followed by the elimination of Methanol and combustion of carbon based materials in the temperature range of 180°C and 364°C and oxidation of Mg at 440°C. TG result showed that mass loss of the dried sample was 23.81%. Our results are comfirm that V.S. Ramachandran et al. (Ramachandran, et al., 2002).

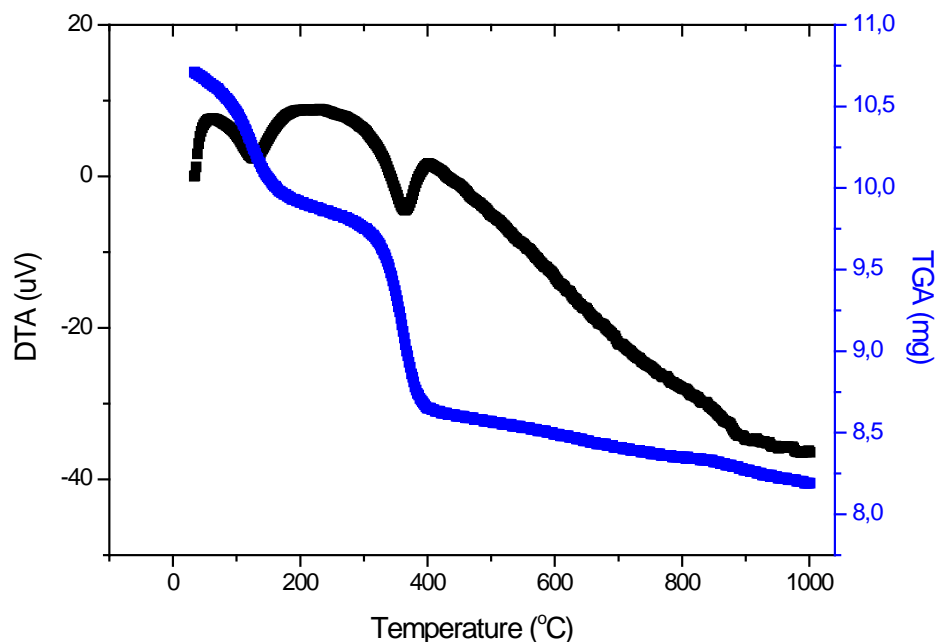


Figure 4.1 DTA and TG curves of Mg based materials dried at 500°C for 2 hours in air

#### 4.2.2 FTIR Analysis

Figure 4.2 presents FTIR spectra of Mg based materials heat treated at 25°C, 100°C, 200°C, 500°C and 600°C for 30 minutes in air. It was found that depending on heat treatment process, organic structure was changed. In these experiments, the analysis was carried out in 650- 4000  $\text{cm}^{-1}$  band range. It is important to realize that the high intensity band at 1500  $\text{cm}^{-1}$  may related with C=C bonds in the matrix from the acedic acid ( $\text{CH}_3\text{COOH}$ ), and the weak bands at 600-700  $\text{cm}^{-1}$  may related with C-H bonds at the room temperature, 100 °C and 200 °C samples. 500 °C and 600 °C experimentation results shown that pure MgO pick on the graphics. Note that upon increasing heat treatment temperature, carbon based bands dissappeared in the samples. Our results are similar to Takenobu Suzuki and etc. results. As seen TG chart confirms that our results.

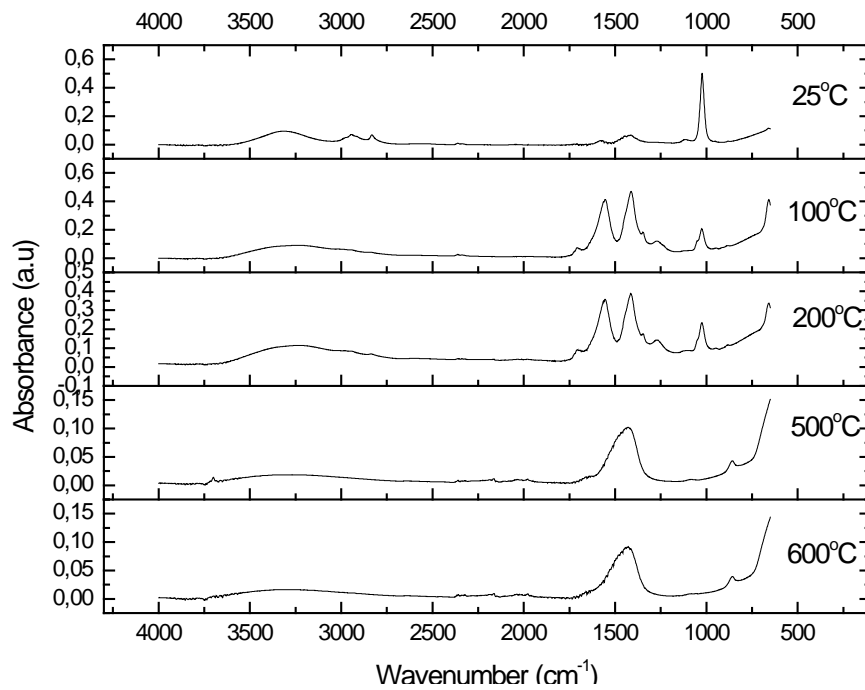


Figure 4.2 FTIR results of Mg based powders heat treated at different temperatures for 30 minutes in air

### 4.2.3 Phase Analysis

XRD pattern of MgO nanoparticles is presented in Figure 4.3. It is found from this result that MgO nanoparticles are periclase phase. Our result is similar to Takenobu Suzuki and etc. results. This phase structure of MgO can be used refractory materials, pharmaceutical industry, glass industry and catalyst in many application areas.

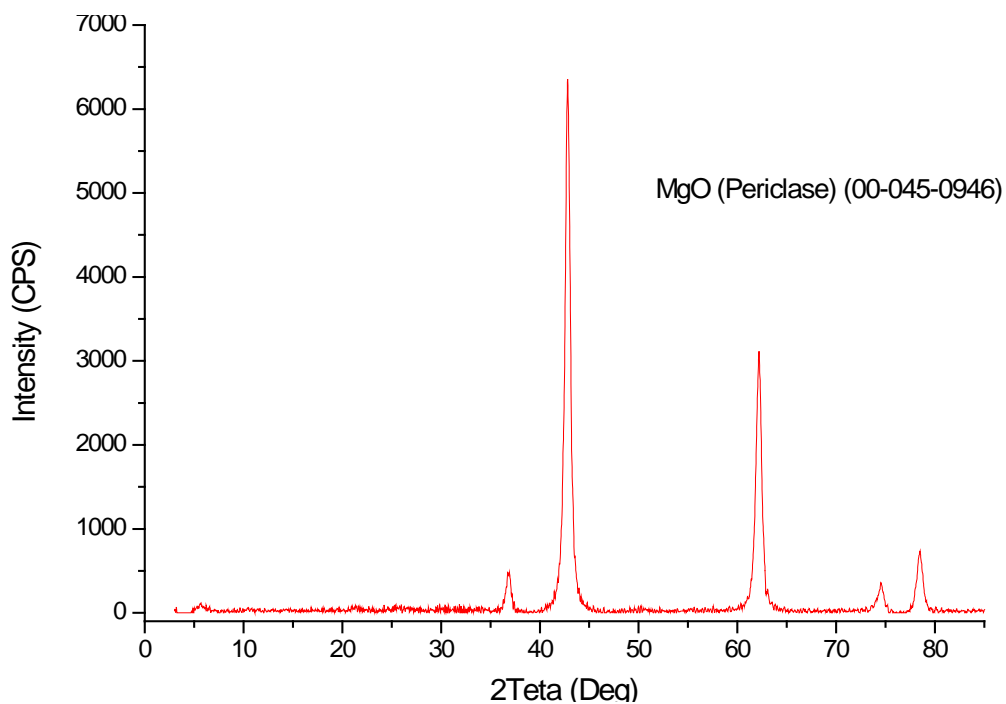


Figure 4.3 XRD pattern of MgO nanoparticles

#### 4.2.4 XPS Analysis

Elemental analyses of MgO nanoparticles were determined with the help of XPS. The XPS analysis of MgO nanoparticles is shown in Figures 4.4, 4.5 and 4.6. Once the result was analyzed, it was determined to be Mg and O elements which belong to MgO nanoparticles. Elemental analysis results of the nanoparticles in Table 4.1 were detected. The element has been found that the rate of 68.78% O and 31.22% Mg as a result of the overall screening. The results are shown that the structure of the compound is MgO. Also the results are confirm from NIST X-ray Photoelectron Spectroscopy Database. (Alexander, et al., 2012).



O1s



Figure 4.4 XPS result of MgO nanoparticles showing 1s elemental scanning for oxygen

Mg1s



Figure 4.5 XPS result of MgO nanoparticles showing 1s elemental scanning for magnesium

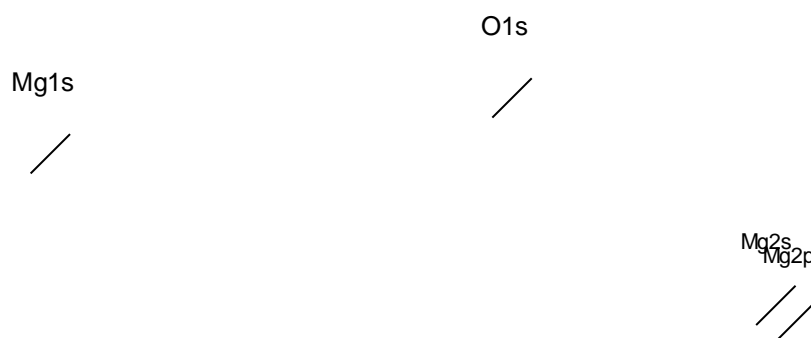


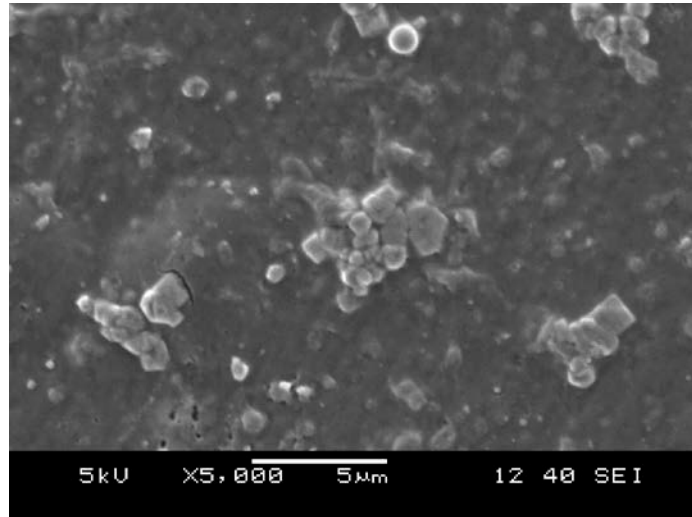
Figure 4.6 XPS result of MgO nanoparticles showing general scanning for the magnesium oxide nanoparticles

Table 4.2 XPS results of MgO particles showing elemental ID and quantification

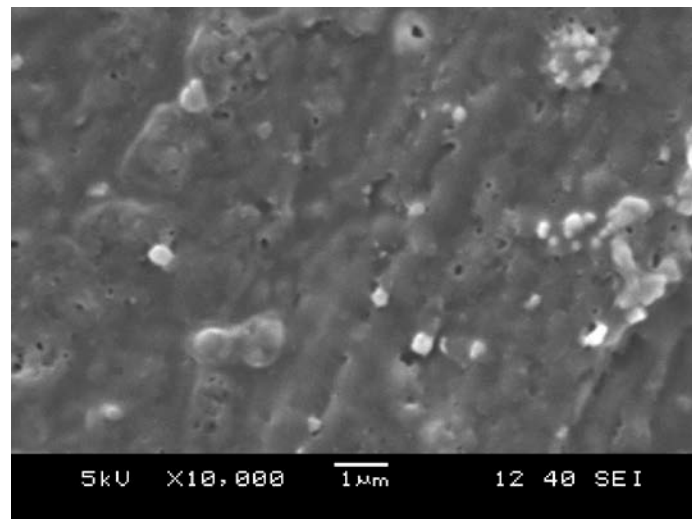
Name	Peak BE	FWHM eV	Area (P) CPS.eV	At. %	Q
Mg1s	1304.64	3.524	300391.13	31.22	1
O1s	532.18	3.461	468823.91	68.78	1

#### 4.2.5 Microstructure

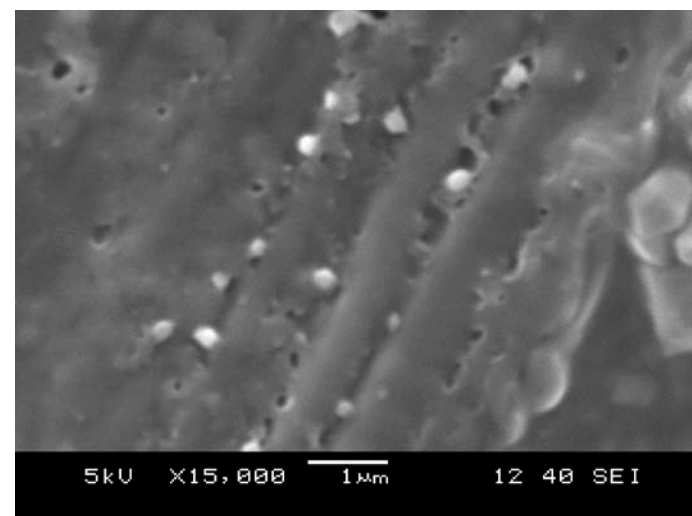
In order to examine the surface properties of MgO nanoparticles, SEM micrographs at different magnifications were taken and shown in Figure 4.7. It is clear from these figures that MgO nanoparticles are nano-sized and well rounded and seems to be agglomerated with each other.



(a)



(b)



(c)

Figure 4.7 SEM images of MgO nanoparticles ( a) 5.000X, (b) 10.000X and (c) 15.000X

#### 4.2.6 Particle Size Distribution

Before flame spray pyrolysis process, particle size distribution of MgO particles is shown in Figures 4.8. As a result of the particle size analysis, particle size distribution ranged from approximately 70-150 nm. The average particle size of MgO powders was found to be 121 nm. This wide range in the graphic is because of agglomerated particles. Also the particles are not dispersed.

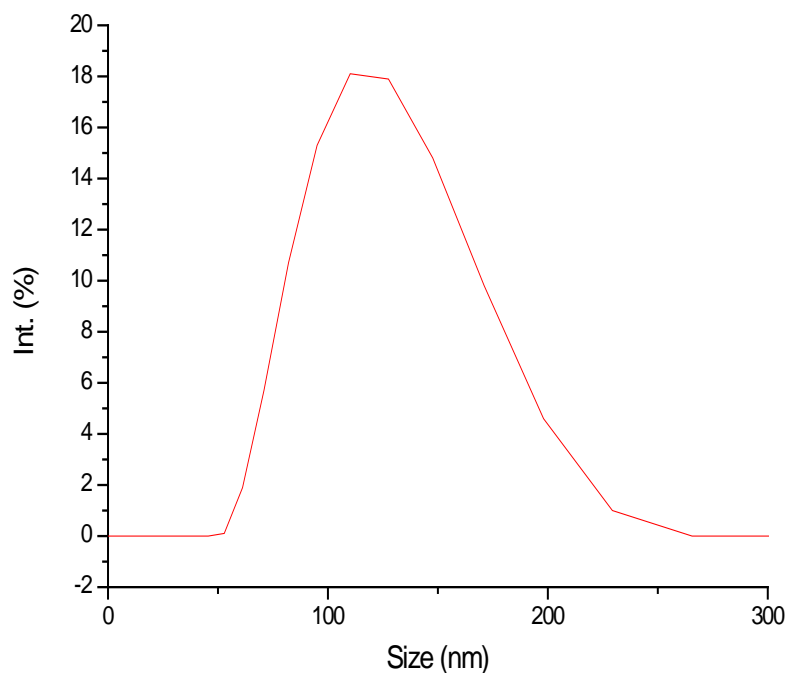


Figure 4.8 Particle size distribution of MgO nanoparticle

## CHAPTER FIVE

### CONCLUSIONS AND FUTURE PLAN

The prefix *nano* in the word *nanotechnology* means a billionth ( $1 \times 10^{-9}$ ). Nanotechnology deals with various structures of matter having dimensions of the order of a billionth of a meter. While the word *nanotechnology* is relatively new, the existence of functional devices and structures of nanometer dimensions is not new, and in fact such structures have existed on Earth as long as life itself.

Magnesium oxide (MgO) is a versatile oxide material according to its broad applications, such as in catalysis, hazardous waste treatment, antimicrobial materials, refractory materials, and superconductor materials. The most conventional method for MgO synthesis is via the thermal decomposition of several magnesium salts.

Magnesium oxides are used in a variety of industrial applications, e.g., as heat-resistant and high-temperature insulating materials, and fuel-oil additives besides as a heat-resistant glass composite in liquid crystal display panels, electroluminescence display panels, plasma display panels, and fluorescent display tubes.

There are several methods for preparing MgO including high-temperature solid state synthesis, sol-gel techniques, and vapor-phase oxidation. Flame spray Pyrolysis is vapor-phase oxidation process.

Flame spray pyrolysis (FSP) is a promising technique for the synthesis of high purity nanosized materials with controlled size and crystallinity in a single step. It was systematically investigated using an external-mixing gas-assisted atomizer supported by six premixed methane-oxygen flamelets. In this study, MgO nanoparticles were produced and characterized using flame spray pyrolysis technique.

Our objective in this study production MgO nanoparticle size material and characterization of this material. After that we want to dop it in the CNT and investigate Solar Energy Efficiency of this material. In this study we used Magnesium Ethoxide for precursor with Methanol Solvent and Acetic Acid. Solution heated up to 100°C with Magnetic Stirrer. After this process the solution given to the FSP for the production MgO nanoparticles. After process nanoparticles collected with the collector spoon.

The synthesized MgO particles were systematically characterized by thermogravimetry and differential thermal (TG-DTA) analysis, X-ray diffraction (XRD) and some more experiments.

Turbidimeter and pH meter were used for blurring and for the solution acidic characterization of the solution. Turbidimeter average 4.42 and pH meter results 6.26. So the solution was clear and acidic as we expected.

DTA-TG and FT-IR were used for the Flame Spray Pyrolysis Process Optimization. The both results shown that the particles are produced was optimum conditions.

XRD, XPS, SEM and Particle analyzer were used for the investigation nanoparticle specifications and the material properties. X-ray diffraction spectrometer (XPS Therm Fischer) was used to analyze the elemental powders structure and lattice. The particles were heated up to 500°C while 2 hours. The XRD Patterns showed that MgO and Periclase MgO generation was observed. This phase structure of MgO can be used refractory materials, pharmaceutical industry, glass industry and catalyst in many application areas. X-ray photoelectron spectrometer (XPS Therm Fischer, Al-K $\alpha$ ) was used to analyze the elemental powders. The element has been found that the rate of 68.78% O element and 31.22% Mg element as a result of the overall screening. The results are shown that the structure of the compound is MgO. The particles is shown nano-sized and well rounded on the 5.000X, 10.000x and 15.000x magnification picture and seems to be agglomerated

with each other. Particle size analyzer was used to determine the size of the particles. Particle size distribution ranged from approximately 70-150 nm. The average particle size were analyzed 121 nm. The reason for this wide range because of agglomerated particles and it is not dispersed.

Future studies we recommended to produce Magnesium Oxide with some dopant Material such as Fe, Ni, Co, Cr for the catalytic experimentation.

## REFERENCES

- Alvarado, E., Torres-Martinez, L.M. & Fuentes, A.F. (2000). Preparation and characterization of MgO powders obtained from different magnesium salts and the mineral dolomite, *Polyhedron*, *19*, 2345-2351
- Ashok, K., Subhash, T., Shikha, V. & Jitendra, K. (2011). Sol-gel synthesis of highly luminescent magnesium oxide nanocrystallites. *Journal of Luminescence*, *131*, 640-648.
- Crist, B.V., (2011). *Handbook of monochromatic XPS spectra*. Chichester: John Wiley & Sons Ltd.
- Ding, Y., Zhang, G., Wu, H., Hai, N., Wang, L. & Qian Y. (2001). Nanoscale magnesium hydroxide and magnesium oxide powders: control over size, shape, and structure via hydrothermal synthesis. *Chemistry Materials*. *13*, 435-44
- Ehre, D., Elazar, Y. & Chaim, R. (2005) Densification of nanocrystalline MgO ceramics by hot-pressing. *Journal of the European Ceramic Society*, *25*, 3579-3585.
- Ferro, S. (2012). FYI: Why do libraries have that smell?. *Popular Science*. Retrieved January 19, 2012, from <http://www.popsci.com/science/article/2011-12/fyi-why-do-libraries-have-smell>
- General Chemistry Laboratory. (n.d.) *The Synthesis of Magnesium Oxide*. Retrieved June 29, 2013, from <http://infohost.nmt.edu/~jaltig/MagOxide.pdf>
- Gleiter, H. (1981). Materials with ultrafine grain size. *2nd Riso International Symposium. Metallurgy Material Science*, 15-21.



- Gleiter H. (1989). Nanocrystalline materials, *Progress in Materials Science*. 33: 223–315.
- Goddard, W., Brenner, D., & Lyshevski, S. (Eds.). (2002) *Handbook of nanoscience, engineering, and technology*, United States of America: CRC Press.
- Hong, Y.C. & Uhm, H.S. (2006). Simulated experiment for elimination of air contaminated with odorous chemical agents by microwave plasma burner. *Chemical Physics Letters*, 422,174.
- Huang, L. & Li, D.Q. (2005). Preparation and bactericidal property of MgO nanoparticles on  $\gamma$ -Al<sub>2</sub>O<sub>3</sub>. *Inorganic Biochemistry*, 99:986.
- Itatani, K., Yasuda, R., Howell, F.S. & Kishioka, A. (1997). Effect of starting particle size on hot-pressing of magnesium oxide powder prepared by vapour-phase oxidation process. *Journal of Materials Science*, 32, 2977-2984
- Jiu, J., Kurumada, K., Tanigaki, M., Adachi, M. & Yoshikawa, S. (2003). Preparation of nanoporous MgO using gel as structure-direct template. *Materials Letters* 58, 44-47.
- Kepler, J., (1611). *Strena seu de Nive Sexangula*. Frankfurt: G. Tampach. ISBN 3-321-00021-0.
- Kirk, R.E., Othmer, D.F., Grayson, M. & Eckroth, D. (1981). *Encyclopaedia of Chemical Technology*, 14, USA: John Wiley and Sons.
- Kresge, C.T., Leonowicz, M.E., Roth, W.J., Vartuli, J.C. & Beck, J.S. (1992). A new family of mesoporous molecular sieves prepared with liquid crystal templates. *Journal of the American Chemical Society*, 114, 10834–10843.

- Kwok, K.S. & Ellenbogen, J.C. (2002). Moletronics: future electronics, *Material Today*, 5, 28–37.
- Laine, R., Marchal, J., Sun H. & Pan, X. (2005). A new Y<sub>3</sub>Al<sub>5</sub>O<sub>12</sub> phase produced by liquid-feed flame spray pyrolysis (Lf-Fsp), *Advanced Materials*, 17, 830.
- Maedler, L., Kammler, H.K., Mueller, R. & Pratsinis, S.E. (2002). Controlled synthesis of nanostructured particles by flame spray pyrolysis, *Journal Aerosol Science*, 33, 369–389.
- MedlinePlus. (2009) *Magnesium oxide*. Retrieved January 2/2009, from <http://www.nlm.nih.gov/medlineplus/druginfo/meds/a601074.html>
- Mark, A. (2006). *The chemistry and technology of magnesia*. USA: John Wiley and Sons.
- Mary, C., Gregory, A., Jerald, R. (1994). *Laboratory Instrumentation*. USA: John Wiley and Sons. ISBN 0471285722.
- McKenna, P. (2010). Emission control: Turning carbon trash into treasure. *New Scientist*, 2779, 48–51.
- McMullan, D. (2006). Scanning electron microscopy 1928–1965. *Scanning* 17(3), 175.
- McMullan, D. (1988). Von Ardenne and the scanning electron microscope. *Microscope Society*, 23, 283–288.
- Morokhov, I.D., Trusov, L.I. & Chizhik, S.P. (1977). *Highly dispersed metallic*. Moscow, Atomizdat Media.

- Nagappa, B. & Chandrappa, G.T. (2007). Defluoridation of bore well water using combustion derived nanocrystalline magnesium oxide. *Microporous Mesoporous Materials*, 106,212.
- Novoselov, K. S., Geim, A. K. & Morozov, S. V. (2004). Electric field effect in atomically thin carbon films. *Science*, 306, 666-669.
- NIST X-ray Photoelectron Spectroscopy Database (Alexander, V., Anna Kraut, V., Stephen, W. & Cedric J.P.) (n.d.). *NIST Standard Reference Database 20, Version 4.1*. Retrieved June 28/2013 from <http://srdata.nist.gov/xps/Default.aspx>
- Parekh Marg, N. & Matunga, M. (2013). Novel and green approach for the nanocrystalline magnesium oxide synthesis and its catalytic performance in Claisen–Schmidt condensation. *Catalysis Communications*, 36, 79–83.
- Park, J.Y., Lee, Y.J., Jun, K.W., Aeg, J.O. & Yim, D.J. (2006). Chemical synthesis and characterization of highly oil dispersed MgO nanoparticles. *Journal Indian Engineering Chemistry*, 12(6),882
- Ramachandran, V.S., Ralph, M., James, J. & Ana, H. (2002). *Handbook of Thermal Analysis of Construction Materials*. USA: Noyes Publications.
- Steno, N. (1669). *De solido intra solidum naturaliter contento dissertationis prodromus*. Italy: Florentiae.
- Strobel, R. & Pratsinis, S.E. (2007). Flame aerosol synthesis of smart nanostructured materials, *Journal Materials Chemistry*, 17, 4743-4756.
- Takato, H., Sunouchi, K., Okabe, N., Nitayama, A. & Hieda, K. (1988). High performance CMOS surrounding gate transistor (SGT) for ultra high density, *International · Electron Devices Meeting*, 222–226.

- Takenobu, S., Yasutake, O. & Takao, T. (2006). Structural and fluorescence properties of Ni:MgO–SiO<sub>2</sub> particles synthesized by flame spray pyrolysis. *Materials Science and Engineering*, 128, 151–155
- Tatekawa, Y., Nakatani, K. & Ishii, H. (1996). Small bowel obstruction caused by a medication bezoar: report of a case. *Surgery Today*, 26 (1), 68–70.
- Tellex, A. & Waldron, R. (1955). Reflectance of magnesium oxide. *The Journal of the Optical Society of America*, 45 (1), 19.
- Thermal Laminating Films. (n.d.) *Haze*. Retrieved September 29, 2013, from <http://www.thermallaminatingfilms.com/haze.php>
- Uchida, K., Koga, J., Ohata, A. & Toriumi, A. (1999). Silicon single-electron tunneling device interfaced with a CMOS inverter, *Nanotechnology*, 10, 198–200.
- Venkateswara, K. & Sunandana, C.S. (2007). Structure and microstructure of combustion synthesized MgO nanoparticles and nanocrystalline MgO thin films synthesized by solution growth route. *Journal of Materials Science*, 43, 146-154.
- Wang, W., Qiao, X., Chen, J. & Li, H. (2007). Facile synthesis of magnesium oxide nanoplates via chemical precipitation. *Materials Letters*, 61, 3218–3220.
- Wikianswers. (n.d.) *Describe the working principle of a pH meter and pH electrode?*. Retrieved June 29, 2013, from [http://wiki.answers.com/Q/Describe\\_the\\_working\\_principle\\_of\\_a\\_pH\\_meter\\_and\\_pH\\_electrode](http://wiki.answers.com/Q/Describe_the_working_principle_of_a_pH_meter_and_pH_electrode)
- Yang, C.M. (1999). Nanorod-Superconductor Composites: A Pathway to High Critical Current Density Materials, *Science*, 273, 1836-1840

Zhang, Y., Tan, Y.W., Stormer, H.L. & Kim, P. (2005). Experimental observation of the quantum Hall effect and Berry's phase in graphene. *Nature*, 438, 201–204.